01 Feb 2022

Experimental Study of Transport Behavior of Swellable Microgel Particles in Superpermeable Channels for Conformance Control

Yang Zhao

Baojun Bai
Missouri University of Science and Technology, baib@mst.edu

Recommended Citation

Y. Zhao and B. Bai, "Experimental Study of Transport Behavior of Swellable Microgel Particles in Superpermeable Channels for Conformance Control," *SPE Journal*, vol. 27, no. 1, pp. 790 - 805, Society of Petroleum Engineers (SPE), Feb 2022.
The definitive version is available at https://doi.org/10.2118/208576-PA

Experimental Study of Transport Behavior of Swellable Microgel Particles in Superpermeable Channels for Conformance Control

Yang Zhao and **Baojun Bai***, Missouri University of Science and Technology

Summary

Gel treatment is an effective way to attack excessive water production during oil development. The transport behavior of gel materials in reservoirs is of crucial importance to the effectiveness of gel treatments. The aim of this paper is investigating the transport behavior of swellable micrometer-sized preformed particle gels (PPGs, or microgels) through superpermeable (super-K) channels. Sandpacks with permeabilities ranging from 27 to 221 darcies were used to mimic the super-K channels. Multiple pressure sensors were applied along the sandpack models to monitor the propagation behavior of the microgels. The tested microgel particles could transport through the super-K channels, and a higher driving pressure gradient was required when the particle/pore size ratio was larger. The pressure gradient distribution along the super-K channels was relatively uniform when the particle/pore ratio was low (less than 1.3). However, the inlet section would show increasingly higher pressure gradients as the particle/pore ratio was increased, indicating increased difficulty in propagation. The propagation of the gel particles was significantly slower compared with the carrying fluid. The delayed propagation behavior was more pronounced when the particle/pore ratio was higher. The injection pressure was much less sensitive to the injection flow rate compared with a Newtonian fluid. The gel dispersion exhibited an apparent shear thinning (pseudoplastic) behavior when transporting through the porous channels. Breakage of the gel particles was observed especially at high superficial velocities. The particle breakage was partially responsible for the apparent shear thinning behavior. The breakage phenomenon was in favor of deep placement of the gel particles. The channel permeabilities were significantly reduced by the microgels, bringing sufficient resistance to subsequent waterflooding (more than 99.5%). At given matching size conditions, softer gels were more likely to establish in-depth placement and uniform water blocking capacity in the channels. The microgel particles exhibited salinity-responsive behavior to the post-brine flush. The gel particles could shrink and reswell according to the salinity of the injected water. Possibilities were discussed to use this salinity-responsive behavior. Also, the microgels exhibited a particular disproportionate permeability reduction (DPR) effect. After gel injection, the channel permeability to water flow was reduced by more than 20 to 92 times of the permeability to oil flow. This work provides important support to understand the transport behavior of gel particles in super-K channels. The achievements are helpful for gel product selection and gel treatment design.

Introduction

A better oil recovery performance is always the pursuit of the oil and gas industry. However, many challenges are involved. One common problem plaguing many oil and gas fields around the world is the presence of high-permeability channels in the reservoirs. Generally, the channels can be divided into two categories: open fractures and porous-medium-type channels **(Fig. 1).** The channels are beneficial and desirable in some situations (e.g., hydraulic fractures in developing shale gases) because they largely increase the contact areas with the matrices and thus improve the injectivity/productivity. However, in many oil and gas reservoirs, the super-K channels can cause fast breakthrough of the flooding fluids (water, polymer solutions, CO_2, etc.) from the injection wells to the production wells (Seright et al. 2003; Sydansk and Romero-Zeron 2011; Bai et al. 2013). A large portion of oil in the matrices is left unswept, resulting in poor sweep efficiency and unsatisfactory oil recovery performance (Fig. 1). In addition, the excessive production of the flooding fluids also brings economic and environmental concerns (Chang et al. 2020; Dhaliwal et al. 2021). Over the years, many efforts have been made to solve the unwanted channeling problem. Gel treatment has proved to be an effective technique to solve the channeling issue (Seright et al. 2003; Bai et al. 2008, 2015; Aldhaheri et al. 2020, 2021; Kang et al. 2021). Different types of gel systems have been developed and applied: in-situ gels (Sydansk and Romero-Zeron 2011), preformed bulk gels (Seright 1997), and PPGs (Pyziak and Smith 2007; Bai et al. 2007a, 2008, 2012; Larkin and Creel 2008; Vasquez et al. 2008; Peirce et al. 2014; Targac et al. 2020).

This study focuses on the porous-medium-type channeling issue. In this scenario, the preformed bulk gels or normal millimeter-sized PPGs are unlikely to work because of low injectivity in such conditions (Seright 1999a; Elsharafi and Bai 2013, 2016; Imqam et al. 2016). For example, Seright (1999a) observed that an impractically high injection pressure gradient (greater than 200 psi/ft) was required to force the preformed bulk gel [Cr(III)-acetate-HPAM] into a 28-darcy sandpack, which mimicked a proppant-filled fracture. When using in-situ gels, the water- or polymer-solution-like gelant can cause damage to the oil zones (Seright and Brattekas 2021; Zhao et al. 2021a). Therefore, an effective strategy is required to solve this type of channeling issue.

In this work, we tested the feasibility of micrometer-sized PPGs in super-K channels. Due to the special properties of the microgel particles, such as elasticity (deformation), swelling, shrinking, reswelling (i.e., hydration, dehydration, rehydration), and breakage into smaller particles caused by mechanical shear, the gel particles would exhibit complex behaviors when transporting through the repeated convergent-divergent flow channels in porous media. Many factors coexist and interact with each other. The factors include particle-to-pore matching size ratio, gel strength (e.g., the elastic modulus), particle size distribution, particle concentration, phase distribution in the porous medium (e.g., presence of residual oil), and surface charge conditions (for very small particles). The complex flow path geometries make the transport and retention behavior much more complicated.

A brief literature survey is summarized here to illustrate the progress achieved over the years. Note that the survey is not exhaustive, because a thorough review is not the objective of our current work. The gel particles could directly pass through the pore throat larger

*Corresponding author; email: baib@mst.edu

Original SPE manuscript received for review 12 July 2021. Revised manuscript received for review 30 July 2021. Paper (SPE 208576) peer approved 3 August 2021.

than themselves because of the deformability nature of the gel particles (Bai et al. 2007b). At higher driving pressures/forces, the gel particles could shrink or even break into small pieces and thus pass pore throats that were much smaller than themselves. For example, Bai et al. (2007b) observed that the gel particles in their study could pass through a microchannel that was only approximately one-quarter of the gel particle size. It was also reported that the particles could be retained in the porous media by different mechanisms. The particles could be adsorbed on the pore surfaces due to the surface charges, which was more prominent because the particles were significantly smaller than the pores (Chauveteau et al. 2003; Yao et al. 2017). For a swarm of particles, the interparticle interactions made the system more complex. For instance, the particles could block a pore throat by a bridging effect or by forming a particulate filtration layer (Yao et al. 2020).

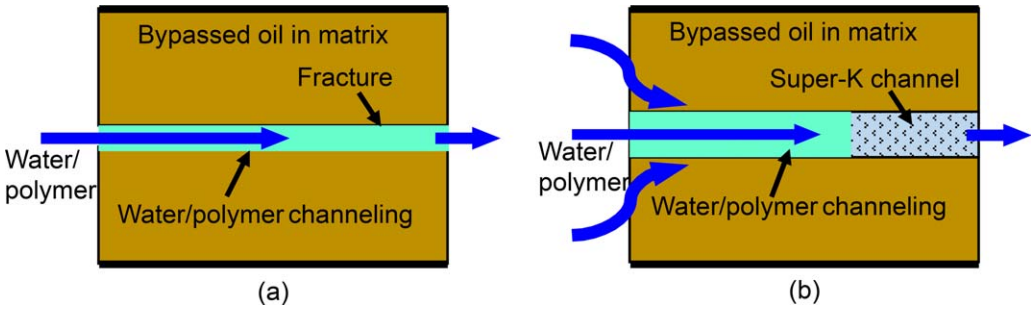

Fig. 1—(a) Open-fracture-type channel and (b) porous-medium-type channel in a reservoir. This channel is composed of pore-throat structures. Preformed bulk gel and the normal PPG are difficult to inject into and shut off the channel. Micron-sized gel particles (microgel) are likely to work and solve this kind of channeling problem.

Yao et al. (2012) observed that the particle/pore size ratio had a significant impact on the transport behavior and thus on the water blocking efficiency of their elastic microspheres (4.3 to 40 μm). Optimal water blocking efficiency was observed at the size ratios of 1.35 to 1.55. When this matching ratio was too small, effective plugging could not be established because of smooth transport and insufficient retention of the microspheres in the porous media. When the matching ratio was too high, the microspheres could hardly penetrate an appreciable depth into the porous media. Thus, the water-plugging efficiency was unsatisfactory. Three plugging mechanisms of microspheres at pore throats were proposed: capture plugging; superposition plugging, and bridge plugging (Yao et al. 2014). They further studied the effects of flow rate, pore-throat size, particle size, and injection concentration on transport and retention patterns (Yao et al. 2020). Five transport and retention patterns were observed in convergent-divergent microchannels: surface deposition, smooth passing, direct interception, deforming remigration, and rigid blockage. Al-Ibadi and Civan (2013) reported that pore-throat plugging and pore-surface deposition were the main blockage mechanisms of gel particles. Zhao et al. (2014) proposed that the dispersed particle gel developed could reduce the permeability of channeling zones by adsorption, retention, trapping, and bridging. They also observed the DPR phenomenon in the water and oil phases after the gel treatment. Farasat et al. (2017) performed a series of coreflooding experiments using limestone grain packs to investigate the retention (mechanical entrapment) behavior of PPGs in porous media. Imqam et al. (2018) studied the effect of different factors on the transport behavior of microgels in unconsolidated sandpack cores. Four transport patterns were reported: plugging, high retention, breaking, and pass; high retention and pass; and low retention and pass.

Numerical studies help get a better understanding of the transport mechanisms of deformable gel particles in porous media. Liu et al. (2017) numerically studied the transport behavior of deformable gel particles based on size-exclusion theory. Zhou et al. (2017) used an improved lattice Boltzmann-discrete element simulation method to study the transport behavior of soft gel particles in porous media. They numerically investigated the effect of particle/pore size ratio and particle strength on the critical pressure gradient for a single gel particle transport through a single pore throat. They reported an exponential relationship between the critical pressure gradient and the size ratio and linearly correlated with the elastic modulus. For the single particle transport process, they observed that the flow rate had negligible impact on the critical pressure gradient. Goudarzi et al. (2015) reported transport behavior of PPGs in fracture and sandpack models. The potential of PPGs in improving the conformance and suppressing excessive water production was investigated. They developed a set of models to characterize the gel rheology, adsorption, swelling ratio, resistance factor, and residual resistance factor of the PPGs in fracture and porous media (sandpacks). The models were incorporated into a reservoir simulator (UTGEL, University of Texas, Austin, Texas, USA). They validated the gel transport models with experimental results, yet some important phenomena, such as dehydration, particle breakage, and surface plugging, were not considered in the models.

Overall, although significant progress has been achieved with the efforts of various researchers, a better understanding is still required regarding the deformable microgel transport in porous media, as pointed out by some recent review papers (Villone and Maffettone 2019; Leng et al. 2021; Wu et al. 2021). The first-ever polymer-flooding project has been ongoing to tap the tremendous heavy oil resources on Alaska's North Slope (Dandekar et al. 2019, 2021a, 2021b; Ning et al. 2020). Conformance control is an important issue to improve the effectiveness of polymer flooding in heavy oil reservoirs (Zhao et al. 2021a). In this study, sandpacks prepared with silica sand were used as the super-K channels to investigate the propagation behavior of microgel particles. Multiple pressure sensors were applied along the sandpack models to monitor the propagation dynamics. Chase brines with different salinities were injected after the gel treatment to test the water blocking performance. Crude oil was also injected to study the different blocking abilities of the microgels to water flow and to oil flow.

Experimental

Materials. ***Brines.*** Two brines were prepared in the laboratory based on the brine composition in the Milne Point oil field on Alaska's North Slope **(Table 1).** The synthetic formation brine had total dissolved solids of 27,500 ppm, and the synthetic injection brine had total dissolved solids of 2,498 ppm (Zhao et al. 2021b). At Milne Point, the injection brine was from a low-salinity water resource, and it was used in waterflooding and polymer flooding. The formation brine was used to saturate the sandpacks. Except otherwise noted, the injection brine was used as the initial and post-injection brine, as well as the carrying fluid of the microgels.

Name	Composition (ppm)
Formation brine (synthetic Milne Point formation brine; total dissolved solids = 27,500 ppm)	Na^+: 10,086.0 K^+: 80.2 Ca^{2+}: 218.5 Mg^{2+}: 281.6 Cl^-: 16,834.4
Injection brine (synthetic Milne Point injection brine, total dissolved solids = 2,498 ppm)	Na^+: 859.5 K^+: 4.1 Ca^{2+}: 97.9 Mg^{2+}: 8.7 Cl^-: 1,527.6

Table 1—Basic formation brine and injection brine.

Crude Oil. The crude oil was sampled in August 2018, at a wellhead in the Milne Point field (Well B-28, provided by Hilcorp, Alaska). The oil sample was centrifuged to remove water and solids (if any) and filtered through a 0.5-μm filter paper. The viscosity was 202 cp at reservoir temperature (71°F), with an API gravity of 19.0° (0.940 g/mL).

Microgels. The microgels were obtained by grinding millimeter-sized PPGs (Bai et al. 2007a; Zhao et al. 2021a). The microgels had volumetric swelling ratios of 40 and 20 cm^3/cm^3 in the injection brine and formation brine, respectively. The swelling ratio was defined as the ratio of swollen volume after absorbing water to the original volume of the gel. For the dry microgel particles of 170 to 230 mesh (63 to 88 μm), after fully swelling in the injection brine, the gel particle sizes were in the range of 215 to 300 μm, with an average diameter of 260 μm. The sizes were 170 to 240 μm (average of 206 μm) after fully swelling in the formation brine. Dispersions were prepared with a microgel concentration of 1 wt% (dry weight). The two gels were labeled as softer gel and strong gel, respectively. Their storage moduli were approximately 820 and 1,370 Pa, respectively.

Super-K Sandpack Models. Sandpacks were used as the super-K porous media, which mimicked the super-K channels present in reservoirs. The sandpack model (2.5 cm × 50 cm) had multiple pressure taps that were able to monitor the pressures at different locations in the sandpack **(Fig. 2).** The sandpacks were prepared with silica sand with a wet-packing method. Before preparing the sandpack, the sand was mixed with formation brine at a certain sand/brine ratio. The wetted sands were added into the sandpack tube at multiple times. The sandpack was vibrated with a vibration machine to ensure tight and uniform packing of the sand. Afterward, the sandpack was vacuumed and saturated with formation brine. The permeability was estimated by measuring the stable injection pressures at five different flow rates. The sandpack permeabilities ranged from 26.9 to 221 darcies. The basic information of the sandpacks is summarized in **Table 2.**

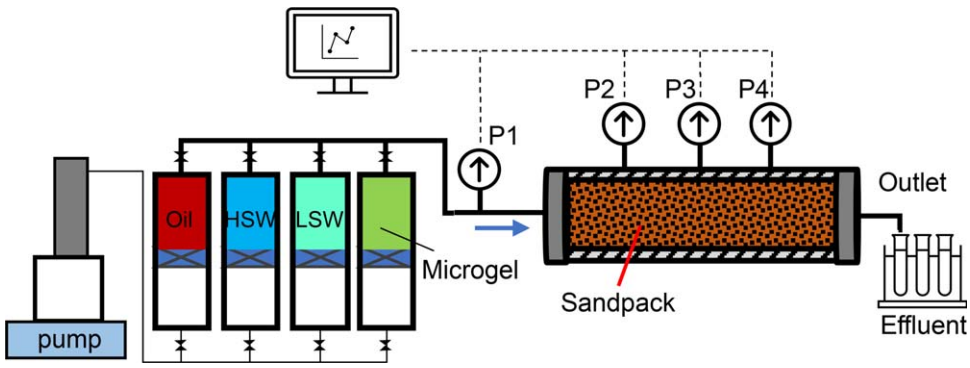

Fig. 2—Experiment setup for microgel transport tests. HSW = high-salinity water; LSW = low-salinity water.

Experiment	*k* (darcies)	Gel Size	Gel Strength	Particle/Pore Ratio	Carrying Fluid
1	55.4	260 (215 to 300)	Soft	2.35	Injection brine
2*	26.9	260 (215 to 300)	Soft	3.29	Injection brine
3	221	150 (100 to 190)	Strong	0.69	Formation brine
4	62.0	130 (90 to 170)	Strong	1.11	Formation brine
5	62.4	150 (100 to 190)	Strong	1.28	Formation brine
6	59.8	206 (170 to 240)	Strong	1.77	Formation brine

*The dimension of this sandpack was 5 cm × 30 cm. Three internal pressure taps were evenly distributed along the model.

Table 2—Summary of basic information of the experiments.

Experimental Procedures. The experimental setup is shown in Fig. 2. The typical experimental procedure is summarized in **Fig. 3.** After measuring the permeability, a brine tracer test (potassium iodide) was carried out to verify the homogeneity. A typical brine tracer test curve is shown in **Fig. 4.** The quick equilibration of the tracer concentration in the effluent indicated good homogeneity of the sandpack core. Note that several factors could affect the accuracy of the tracer tests, such as the sample size and dead volume. As shown in Fig. 4, the concentration was close to 50% at 1 pore volume (PV) after subtracting a dead volume of 2.5 mL from the cumulative effluent volume. The dead volume (0.03 PV) was small compared with the PV.

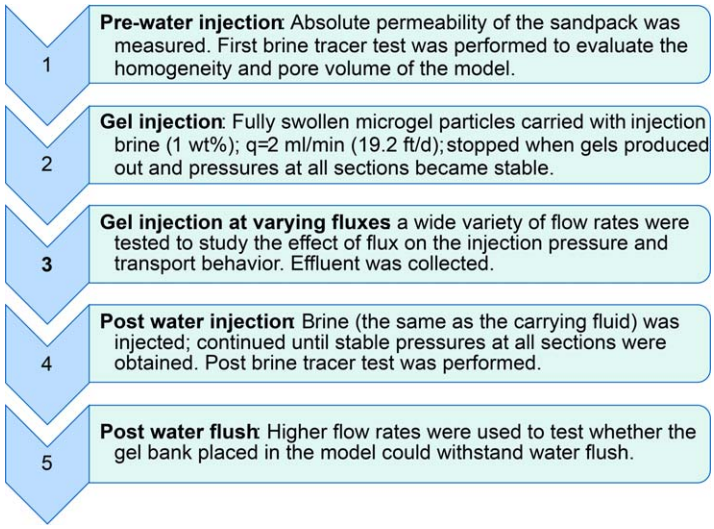

Fig. 3—Typical experimental procedure.

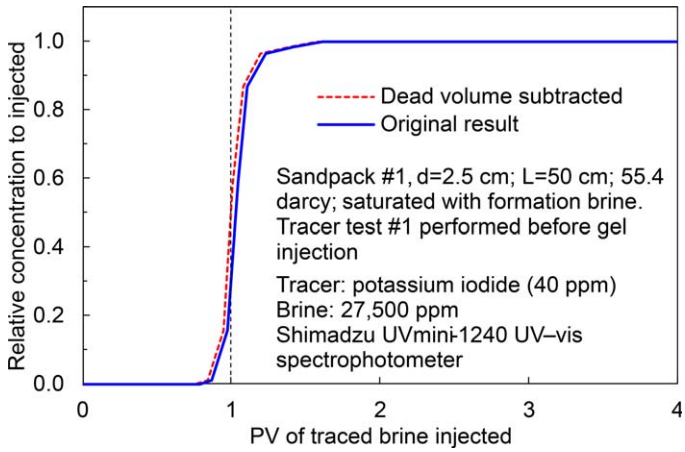

Fig. 4—Results of brine tracer test (Exp. 1, before gel injection). UV-vis = ultraviolet-visible.

The microgel dispersion was injected at 2 mL/min (19.2 ft/D) until stable injection pressures were reached at all the pressure taps. The pressure response was an indication of the gel transport dynamics in the sandpack. The moments when the pressures at different locations began to increase were recorded. The onset of pressure increase indicated that the microgel bank front had arrived at that pressure tap. The gel-dispersion accumulator had a mixing propeller mounted at the bottom to ensure the particles dispersed uniformly in the carrying fluid. In Fig. 2, this accumulator was drawn upside down for simplicity. The effluent was closely monitored to capture the moment when the microgels came out from the outlet.

The effluent was also collected at different flow rates to examine the impact of flow rate on the particle size of the microgels as transporting through the porous media. At the given flow rates, the effluent samples were collected at stable conditions to minimize the impact of the previous flow conditions. The size and morphology of the samples were examined with an optical microscope (HIROX digital microscope KH-8700). Also, the pressures in the sandpacks at different flow rates were monitored. Stable pressures were used to calculate resistance factors (F_r) at different sections in the sandpack. Afterward, chase water was injected at 2 mL/min until stable pressures were reached at all locations. Residual resistance factors (F_{rrw}) at different sections were calculated to evaluate whether the microgels effectively shut off the super-K channels to water flow at the in-depth regions.

Results and Discussion

Transport Behavior of Microgels. Fig. 5 shows the pressures at different locations during the gel injection process along the super-K sandpack in Experiment (Exp.) 1. In this experiment, the average particle/pore ratio in this experiment was 2.35. The specific pressure responses during gel propagation through the model were summarized in **Table 3.** At the beginning, the pressure at the inlet (P1) increased linearly, whereas the other three pressure sensors showed no change (remaining zero), as shown in Fig. 5. After injecting

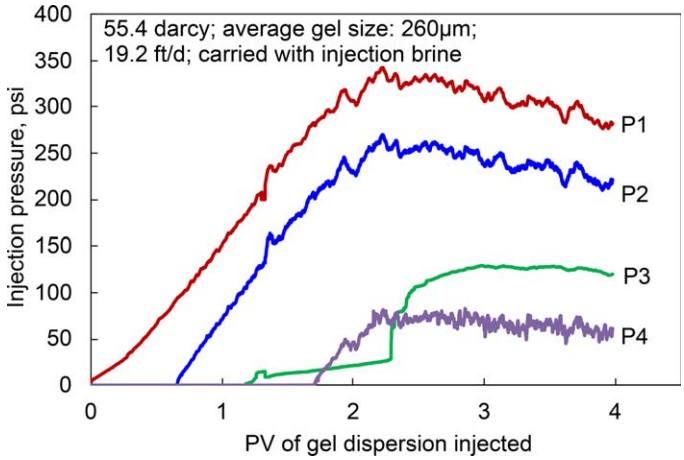

Fig. 5—Pressures at different locations during gel injection (Exp. 1).

Gel Front	*t* (minutes)	Dispersion Injected (mL)	Dispersion Injected (PV)	P1 (psi)	P2 (psi)	P3* (psi)	P4 (psi)
Arrives at Tap 1 (inlet)	0	0.00	0	0	0	0	0
Arrived at Tap 2	28.7	57.40	0.719	93.9	0	0	0
Arrived at Tap 3	51.3	102.60	1.286	183.6	105.8	0	0
Arrived at Tap 4	74.2	148.40	1.860	280.7	203.1	15.8	0
Arrived at outlet	96.8	193.50	2.424	324.7	251.5	95.6	71.1
Stable (end)	158.8	317.60	3.980	301.0	238.4	128.2	59.4

*Readings are not accurate because of sensor connection malfunction.

Table 3—Responses during gel transport in high-permeability porous media (Exp. 1, particle/pore ratio = 2.35).

57.4 mL of gel dispersion, P2 started to increase, indicating that the gel bank front arrived at the first internal pressure tap (P2). The injected gel dispersion corresponded to 0.72 PV of the whole model or 3.13 PV of the transported section (Section 1). Meanwhile, P1 was increased to 93.9 psi (Table 3), and P2 started to increase almost linearly, following the same trend as observed in P1. The gel bank front sequentially arrived at P3 and P4 after injecting 102.6 and 148.4 mL (1.29 and 1.86 PV) of gel dispersion, respectively. After injecting 193.5 mL (2.42 PV) of gel dispersion, the gel bank front broke out at the outlet. At this moment, the pressures at the four points did not reach stable conditions. Instead, they still increased as more gel dispersion was injected. The pressures at different locations gradually became stable with fluctuations around certain values (301, 238, 128, and 59 psi, respectively). In total, 317.6 mL (3.98 PV) of gel dispersion was injected. The pressure gradients in different sections of the sandpack were estimated, as shown in **Fig. 6.** In each section, the pressure gradient first increased to a peak, and then it gradually decreased and became relatively stable with fluctuation. The fluctuation was a result of repeated accumulation and release/remigration of the microgel particles in the pore-throat structures (Zhao et al. 2021a). The pressure gradients in different sections were comparable with each other. The final stable pressure gradients were in the range of 155 to 249 psi/ft. Because of connection malfunction of Pressure Sensor 3 in the early stage of gel injection, the readings of P3 were not accurate. Instead, the second and third sections were regarded as a whole, and P2 and P4 were used to calculate the pressure gradient in this combined section. The malfunction issue was resolved later, and late-stage P3 was used when calculating the resistance factors.

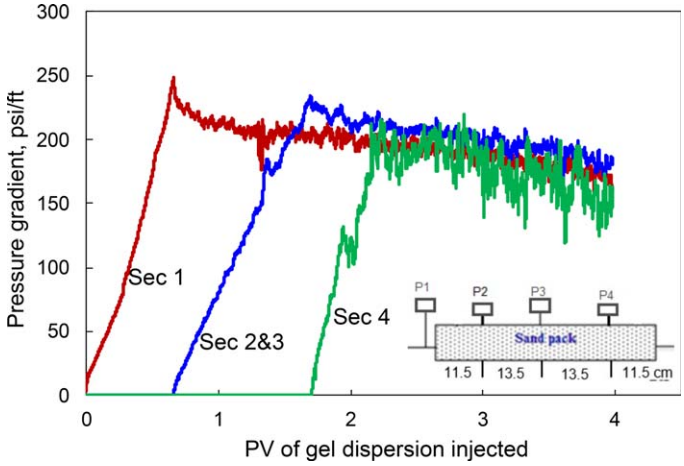

Fig. 6—Pressure gradient at different sections during gel injection (Exp. 1). Sec = section.

With the pressure data, we obtained the resistance factors (F_r) during the gel injection with Eq. 1. The resistance factor is equal to the ratio of pressure gradient during gel injection to the initial brine injection at the same flow rate. The resistance factors in the different sections were shown in **Fig. 7.** The stable resistance factors at different sections of the sandpack are summarized in **Fig. 8.** The resistance factors followed a similar trend as the pressure gradients during the gel injection process. The resistance factors were relatively uniform in all the sections of the model, in the range of 2,216 to 3,549. No progressive surface plugging was observed during the whole process.

$$F_r = \frac{\lambda_w}{\lambda_{\text{gel}}} = \frac{\Delta P_{\text{gel}}}{\Delta P_{\text{initial-water}}}. \quad (1)$$

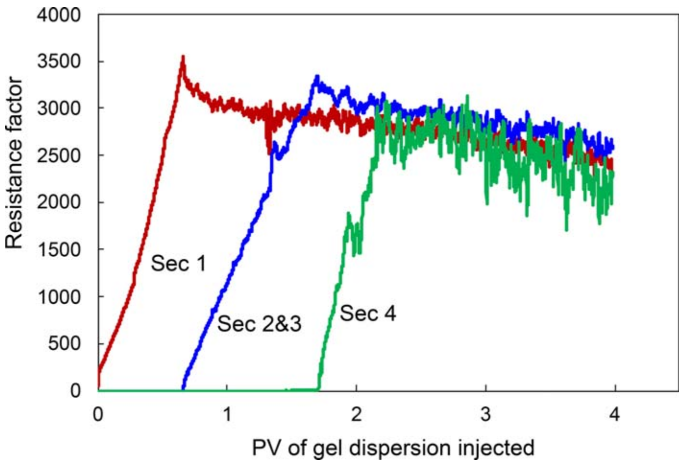

Fig. 7—Resistance factor distribution (Exp. 1). Sec = section.

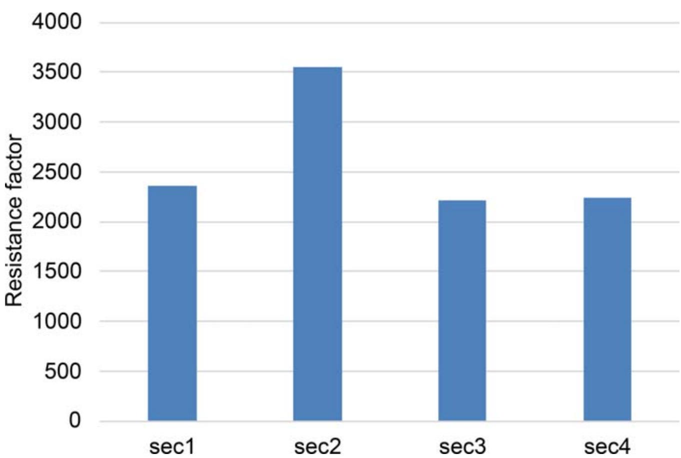

Fig. 8—Stable resistance factor distribution (Exp. 1). sec = section.

In Exp. 2, the particle/pore ratio was 3.29. The pressures, pressure gradients, and resistance factors are shown in **Figs. 9 through 12.** The gel propagation dynamics are summarized in **Table 4.** In this experiment, 1.09 total PV (4.36 local PV) of gel dispersion was injected when P2 started to show response. The propagation speed of the gel particles was obviously slower than that in Exp 1 (4.36 PV vs. 3.13 PV), indicating higher retention of the gel particles in the inlet section because the particle/pore ratio was higher (3.29 vs. 2.35). In total, 770 mL (4.7 PV) of gel dispersion was injected. The stable pressures at the four locations were 361, 213, 130, and 89 psi, respectively. The first section showed a higher stable pressure gradient and resistance factor at the end of the gel injection compared with the values in the in-depth sections. The final stable pressure gradients were in the range of 168 to 602 psi/ft and were obviously higher than that in Exp. 1. It was more difficult for the gel particles to transport and place in the super-K channels because the particle/pore ratio was larger.

The results indicated that although the tested 260-μm microgel particles could be injected into the in-depth sections of the sandpack with a particle/pore ratio of 3.29, high-pressure gradients were required. Such high-pressure gradients are only available in the near-wellbore regions. A particle/pore ratio of 3.29 is not favorable for gel transport and placement in the super-K porous channels. In Exp. 1, the pressure gradients were also too high, although the distributions of pressure gradients and resistance factors were more uniform.

Effect of Particle/Pore Ratio on $\mathbf{F_r}$ ***Distribution.*** More experiments were performed with lower particle/pore ratios to explore the favorable working conditions of the microgel particles. In this study, we used the Carman-Kozeny equation (Eq. 2) to estimate the average pore size of the super-K sandpacks (Carman 1956; Mauran et al. 2001). In this equation, d is the average diameter of the pores (μm), k is the permeability (μm^2) of the core, f_{CK} is the Carman-Kozeny shape factor, τ is the tortuosity, and Φ is the porosity (fraction). A value of 4.5 for the $f_{CK} \times \tau^2$ was adopted in the calculation (Carman 1956; Mauran et al. 2001).

$$d = \sqrt{\frac{16 k f_{CK} \tau^2}{\Phi}}. \quad (2)$$

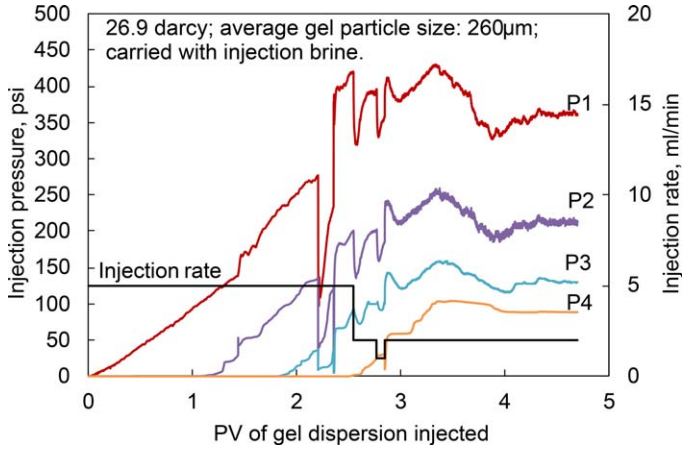

Fig. 9—Injection pressure at different locations during gel injection (Exp. 2). sec = section.

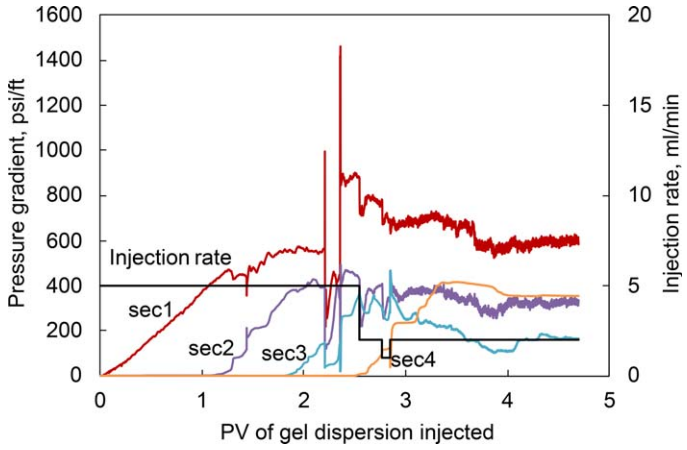

Fig. 10—Pressure gradient at different sections during gel injection (Exp. 2). sec = section.

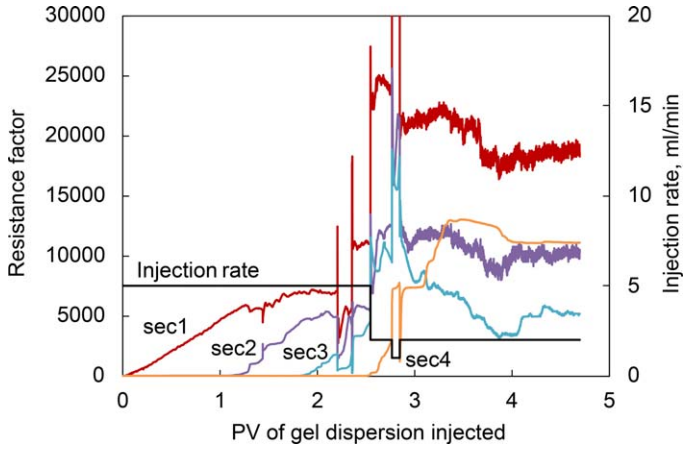

Fig. 11—Resistance factor distribution (Exp. 2). sec = section.

A parameter termed as the relative resistance factor was introduced to describe the surface retention/plugging tendency of the microgel particles in super-K channels. It was the ratio of the resistance factor in the inlet section to the average value in the in-depth sections. A higher value meant a higher retention in the inlet section and thus poorer migration ability into the in-depth sections of the porous channels. In this study, the first section of the sandpacks was regarded as the inlet section. The remaining segments of the sandpacks were regarded as the in-depth sections. The relative resistance factors at different particle/pore ratios were summarized in **Fig. 13.** The results suggested that the resistance factor distribution was relatively uniform when the particle sizes were comparable or smaller than the pore-throat sizes. At the same strength, this parameter increased with the particle/pore ratio, indicating reduced injectivity and increased surface plugging tendency as the particle/pore ratio was increased. Significant retention of the particles in the inlet section was expected, and the particles were difficult to transport deep into the sandpacks. The strength of the gel particles also influenced the transport and retention behavior. Softer particles were easier to transport deep into the models, as indicated by the lower relative resistance factors in Fig. 13.

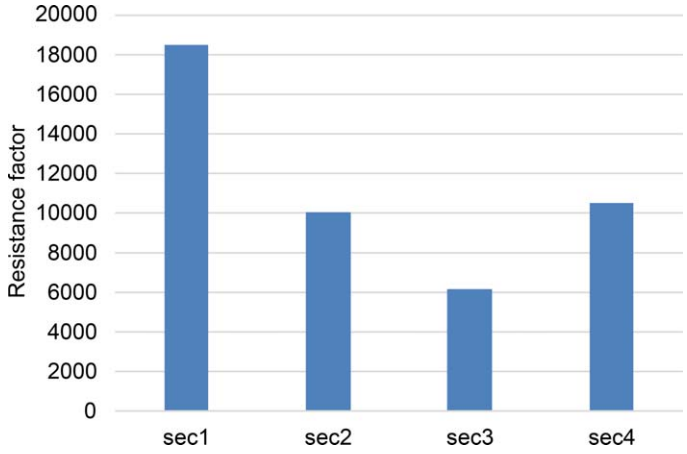

Fig. 12—Stable resistance factor distribution (Exp. 2). sec = section.

Gel Front	*t* (minutes)	Dispersion Injected (mL)	Dispersion Injected (PV)	Flow Rate (mL/min)	P1 (psi)	P2 (psi)	P3 (psi)	P4 (psi)
Arrives at Tap 1 (inlet)	0	0	0	5.0	0	0	0	0
Arrived at Tap 2	35.9	179.25	1.09	5.0	103.2	0	0	0
Arrived at Tap 3	59.3	296.50	1.81	5.0	225.9	86.4	0	0
Arrived at Tap 4	77.9	389.33	2.37	5.0	385.9	168.3	64.5	0
Arrived at outlet	103.0	455.00	2.77	1.0	348.9	180.7	100.0	28.8
Stable	217.5	672.25	4.10	2.0	352.0	207.0	127.0	89.0

Table 4—Responses during gel transport in high-permeability porous media (Exp. 2, particle/pore ratio = 3.29).

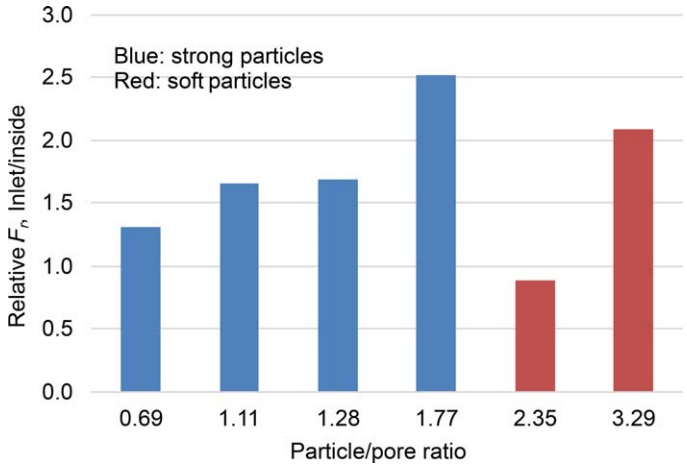

Fig. 13—Resistance factor distribution at different particle/pore ratios.

In addition, the experimental results indicated significant delay of the gel bank front compared with the front of the carrying fluid. **Fig. 14** shows the position of the carrying fluid front and the position of the gel bank front in Exp. 1. The blue line is the assumed ideal case. It was assumed that there was no delay in the gel propagation. That is, the gel would arrive at the outlet after 1 PV of gel dispersion was injected. However, the gel came out after 2.424 PV (green curve). The lag of the gel bank front against the carrying fluid front was caused by the retention of the microgel particles in the porous media. The equilibrium retention was 3,180 μg microgel/g of sand based on material balance by monitoring the amount of gel injected into and produced out of the sandpack model. The volume of the swollen particles in the 2.424 PV dispersion was approximately 1 PV. The red curve represents the propagation distance of the gel when a given volume of swollen gel particles was injected. In the experiment, the gel came out when 1 PV of swollen gel was injected. At that time, the gel was expected to occupy all the pore spaces in the sandpack model. For this curve, the horizontal axis shows the PV of swollen gel injected. For the other two curves, the horizontal axis shows the PV of gel dispersion injected. The red curve almost overlaps with the blue curve. This means the gel front showed no delay in terms of the swollen gel injected, but the front was significantly behind the front of the carrying fluid. Note that the existence of inaccessible PV could result in an earlier breakout of the gel bank front. The inaccessible PV was the pore spaces that were too small for the gel particles to access. However, the inaccessible PV was negligible (zero) in this case because the swollen gel front followed almost the same trend as the no-delay ideal case.

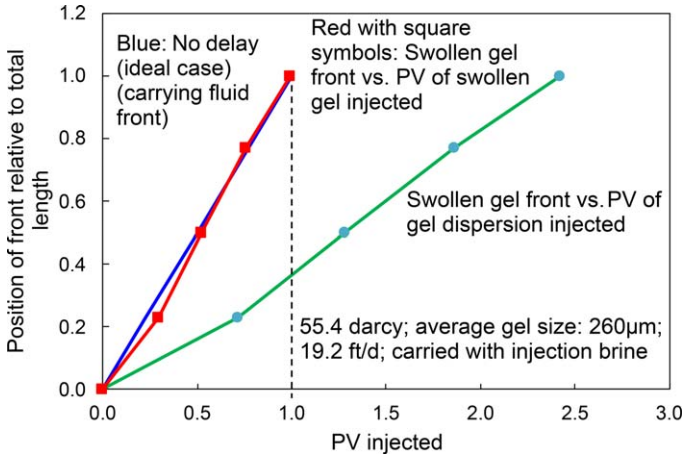

Fig. 14—Transport delay (Exp. 1).

The results also indicated that gel dehydration was not significant because the gels arrived at the outlet after 1 PV of swollen gels was injected (red curve in Fig. 14). In this work, dehydration means the swelled gels lost the absorbed water, whereas the loss of free water from the gel dispersion was not regarded as dehydration. The gel particles shrunk as a result of dehydration, and the loss of free water did not cause shrinkage of the gels. The insignificant dehydration behavior was substantially different from the observations of preformed gel extrusion through fractures (Seright 1997, 1999b, 2001). For the latter cases, as reported by Seright (1997, 1999b, 2001), the gels were significantly dehydrated when extruding through the fractures. The gels were concentrated. The lost water leaked off into adjunct matrices from the fractures. The different dehydration behavior in the present work could be ascribed to the fact that (1) the models were homogeneous sandpacks, and (2) abundant free water was present in the dispersion. The leakoff mechanism present in fracture models (Seright 1999a) was eliminated in homogeneous sandpacks. The gel particles may lose water (dehydrated or squeezed) when extruding through narrow throats. The water was squeezed downstream. However, because free water was available, the particles could absorb water (reswell) after passing the narrow throats. The dehydration and reswelling events occurred repeatedly. On the macroscale, as mentioned in the last paragraph, the gels arrived at the outlet after 1 PV of swollen gel was injected (red curve in Fig. 14). At this moment, 2.424 PV of dispersion was injected (including 1 PV of gels and 1.424 PV of free water). Similar behavior was observed when gel dispersions with different concentrations (800 and 2,000 ppm) were injected through sandpacks (Imqam et al. 2018). At the moment of gel produced out, a larger volume of dispersion was required when the concentration was lower. However, the injected volumes of the gel particles both were close to 1 PV.

Pressure Gradients and Resistance Factors at Different Superficial Velocities. The pressure gradients and resistance factors at different injection rates (0.1 to 50 mL/min, equivalent to 1 to 500 ft/D) were tested. The pressure gradients were shown in **Figs. 15 and 16.** Although the pressure gradient showed an increasing trend with the injection rate, the increase was much more gradual compared with the flow rate. According to Darcy's law, for a Newtonian fluid with a constant viscosity, the pressure gradient should be proportional to the velocity (flux) with a slope of unity (angle = 45°) in a log-log plot (Fig. 16). However, the slope for the gel dispersion was lower compared with the Newtonian fluid, which indicated a decreasing apparent viscosity of the gel dispersion with the increase of flow rate. Consistently, the resistance factor exhibited a decreasing trend, a behavior analogous to a shear-thinning fluid. Similar strong shear thinning behavior was reported for preformed gels in fractures (Seright 1997).

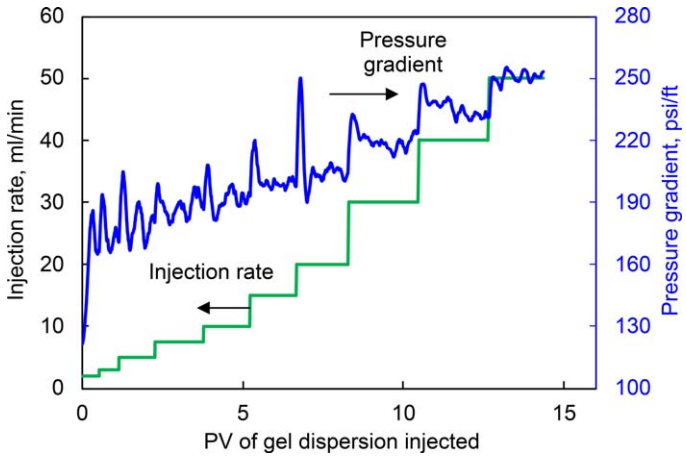

Fig. 15—Pressure gradient at different flow rates.

The decreasing apparent viscosity indicated mechanical degradation was likely to occur when transporting in the porous channels. This hypothesis was supported by microscopy observation of the gel samples collected at different flow rates **(Fig. 17).** Smaller gel particles were observed when the flow rates were higher. The pressure responses also supported this hypothesis; as seen in Fig. 15, when the flow rate increased, the pressure gradient increased at the beginning and then dropped. The changing behavior was in accordance with the breakage of gel particles. The breakage phenomenon is highly related to the significance of the shear force against the strength

of the particles. More severe breakage was observed at higher flow rates for a given microgel material. Therefore, the apparent viscosity (resistance factor) would be reduced. Another possible mechanism responsible for the apparent thinning behavior was the slippage effect (extrusion mechanism) between the gels and the walls of pores. The gels slipped along the pore surfaces and extruded through the pore throats, whereas there was a viscous boundary layer in the case of liquid flow. Seright (1997) reported extrusion behavior of preformed gels through fractures and tubes. The extrusion mechanism was responsible for the observed thinning behavior, especially at high flow rates (Seright 1997).

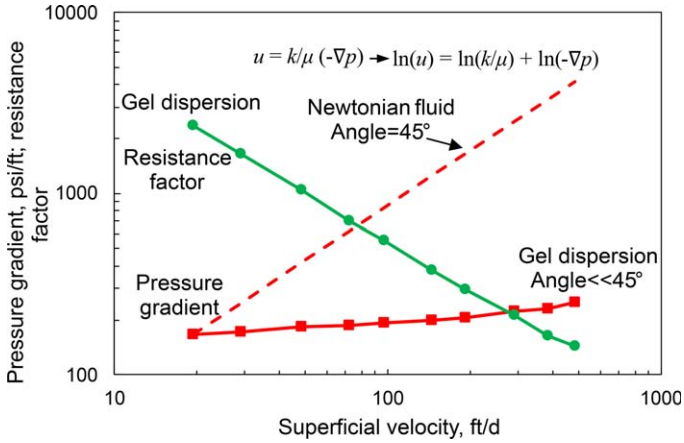

Fig. 16—Pressure gradient as a function of superficial velocity.

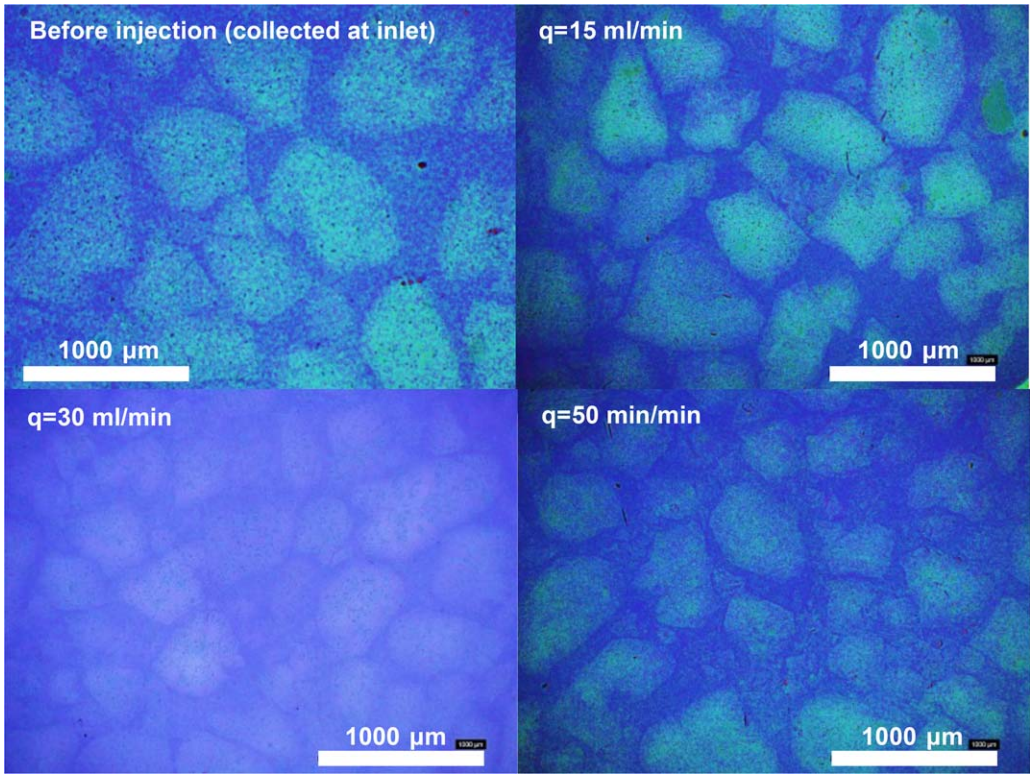

Fig. 17—Microscopy examination of effluent gel samples. (Original particles were collected at the inlet. Effluent samples were collected at 15, 30, and 50 mL/min.)

The particle breakage phenomenon was also reported by other researchers in the literature (Bai et al. 2007b; Farasat et al. 2017; Saghafi 2018; Wang et al. 2017; Li et al. 2019). For instance, Li et al. (2019) observed significant particle size reduction after the microsphere particles transported through an 18-m sandstone core. The broken/pass behavior favored deep penetration of microgel particles under practical pressure gradients. The observed shear degradation (breakage) in this study can partially explain why good injectivity of PPGs was consistently observed in most field applications (Liu et al. 2006; Bai et al. 2008, 2012, 2013). This explanation did not exclude other possibilities, for example, the presence of fractures/super-K channels (e.g., induced by long-term waterflood). The breakage phenomenon would benefit the injectivity of the gel dispersions. On the other hand, however, concerns may rise about the reduced water blocking efficiency as a result of the gel breakage. From a field application point of view, less water blocking ability is required in the in-depth regions of reservoirs. That is, the water blocking efficiency (strength) does not need to be as strong as in the near-wellbore region. Therefore, the particle breakage phenomenon is not supposed to noticeably reduce the overall conformance control performance of the gel treatments.

Transport/Pass Mechanisms. Bai et al. (2007b) reported six transport patterns of particle gels through pore throats on the basis of micromodel experiments, including direct pass, adsorption, deform and pass, snap-off and pass, shrink and pass, and trap. The transport patterns could be estimated based on the pressure response, effluent gel concentration, and gel particle size. The direct-pass pattern was only significant when the gel particle sizes were smaller than the pore size. The adsorption mechanism was only pronounced when the particles were significantly smaller than the pores (Chauveteau et al. 2003; Yao et al. 2017). When the particles were larger than the pore throats (particle/pore ratio > 1), the deform/pass, shrink/pass, and break/pass patterns would coexist. The dominant pattern(s) depended on the flow rate (or driving pressure gradient) for given gel materials. The deform/pass pattern was dominant at low flow rates, whereas the breakage phenomenon was more significant at high flow rates as indicated in Fig. 17. Meanwhile, the retention (entrapment) of the microgels in the channels was high: 3,180 μg/g in Exp. 1. The retention was directly related to the water blocking ability of the microgels.

Water Blocking Performance. The blocking efficiency of the microgels to post-water flow was tested. The same brine used to prepare the gel dispersion was injected at the same flow rate. Stable pressures were reached at the different locations in the models. The results of Exp. 1 are illustrated in **Fig. 18.** The stable pressures were used to calculate the residual resistance factors (F_{rrw}) to the post-waterflood at the different locations **(Fig. 19).** The F_{rrw} was defined as the brine permeability ratios before and after the gel injection, as described by Eq. 3. It was equal to the ratio of brine injection pressures after and before the gel injection.

$$F_{rrw} = \frac{K_{\text{before}}}{K_{\text{after}}} = \frac{\Delta P_{\text{post-water}}}{\Delta P_{\text{initial-water}}}. \qquad (3)$$

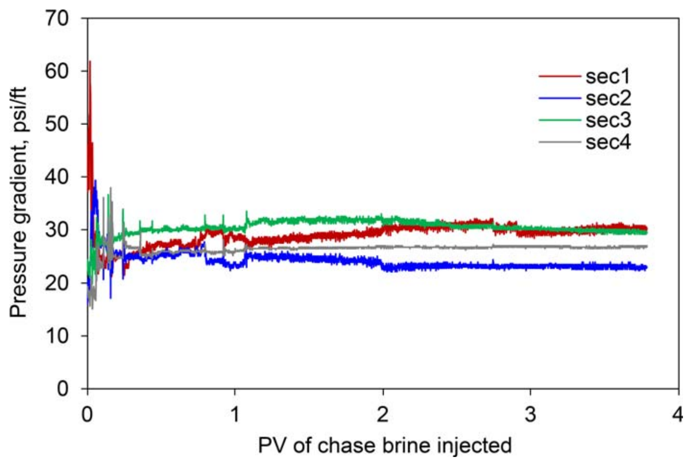

Fig. 18—Pressure gradient during the first chase waterflood (Exp. 1). sec = section.

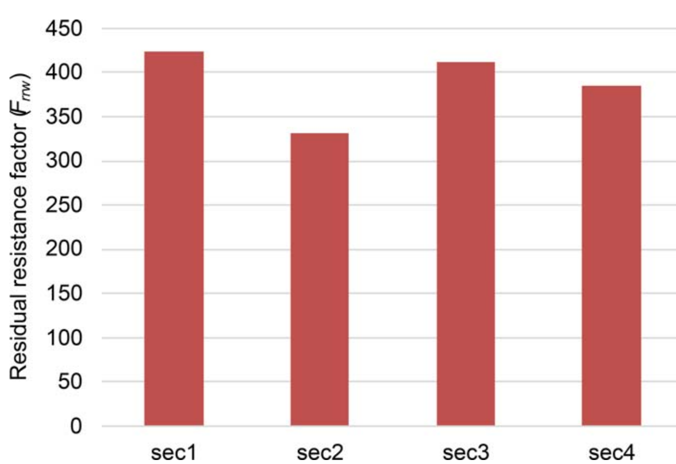

Fig. 19—Distribution of residual resistance factor (Exp. 1). sec = section.

In Exp. 1, the F_{rrw} values after gel injection were in the range of 330 to 420, and the distribution was quite uniform (Fig. 19). No obvious face plugging was detected, as indicated by both the F_r and F_{rrw} distributions (Figs. 8 and 19). Generally, the F_{rrw} distribution was more uniform when the particle/pore ratio was lower, as shown in **Fig. 20.** The relatively uniform distribution of the F_{rrw} indicated uniform retention of the gel particles in the super-K channels. The uniform F_{rrw} distribution was a desirable asset for a deep-profile-control agent. The results demonstrated that the microgel particles were able to effectively establish water blocking efficiency at the in-depth regions of the super-K channels. However, the performance became unsatisfactory when the particle/pore ratio was higher. For example, as the particle/pore ratio increased to 3.29 (Exp. 2), the F_{rrw} in the inlet section was significantly higher compared with the values in the other sections (Fig. 20). This observation agreed with the gel transport behavior as discussed in the preceding subsection. Compared with Exp. 1, the larger diameter/smaller length in Exp. 2 did not make the propagation better. If a smaller length influenced

the propagation, the resistance factors and residual resistance factors in different sections should exhibit a consecutive decreasing trend. The results did not show such a trend (Figs. 8, 12, 19, and 20). Therefore, in the tested conditions (1 to 2 in. in diameter, 1 to 1.7 ft in length), the experiments were not influenced by the larger diameter/smaller length of the sandpacks.

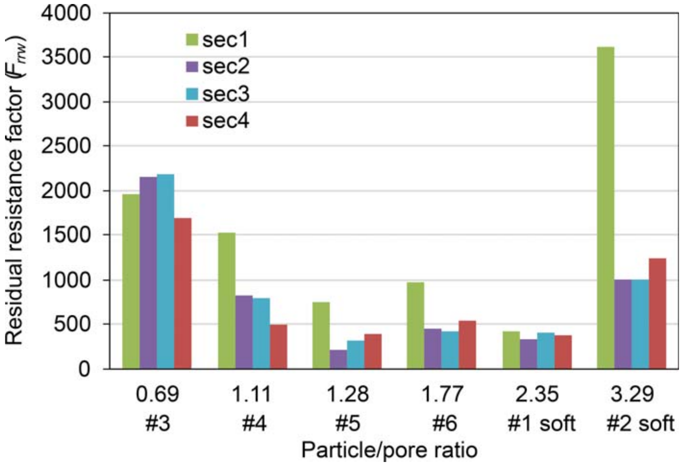

Fig. 20—Summary of residual resistance factor distribution after gel treatment. sec = section.

The results also revealed the impact of strength of the microgels on the water blocking performance (Fig. 20). Comparing Exps. 1 and 6, although the particle/pore ratio of the softer gels was higher than the case of strong gels (2.35 vs. 1.77), the F_{rrw} distribution was more uniform when softer particles were injected. The results suggested that at the same particle/pore ratio conditions, softer gels were more likely to achieve a deep placement and uniform water blocking in the super-K channels.

The results were consistent with our previous observations in microgel conformance control treatment during polymer flooding using channel models (Zhao et al. 2021a). We observed that the critical driving pressure that was required for the microgel particles to penetrate the super-K channels followed a power-law relationship with the permeability of the channel. For the tested microgels, a much higher driving pressure was required because the channel permeability was less than 30 darcies (particle/pore ratio > 3.5), which indicated the ineffectiveness of the microgels under these conditions. The microgels were effective when the channel permeability was greater than 50 darcies (particle/pore ratio < 2.6). Under such conditions, good injectivity, effective water blocking performance, and significant oil recovery improvement were achieved. The results in the current study further confirmed the identified favorable working conditions of the microgels.

The water blocking efficiency (E_{bw}) after gel treatment was estimated with Eq. 4. The E_{bw} values in Exp. 1 were 99.76, 99.70, 99.76, and 99.74% in the four sections. For all the experiments, the water blocking efficiency in the in-depth sections was greater than 99.5%. The lowest value (99.54%) was found in the second section in Exp. 5. The results indicated that the microgels could efficiently shut off the super-K channels. In Eq. 4, K_{before} and K_{after} are the permeabilities of the sandpack to water before and after the gel injection, respectively.

$$E_{bw} = \left(1 - \frac{K_{\text{after}}}{K_{\text{before}}}\right) \times 100\% = \left(1 - \frac{1}{F_{rrw}}\right) \times 100\%. \quad (4)$$

Brine tracer tests after the gel treatment also confirmed that the microgel particles effectively placed in the super-K channel and reduced the effective pore spaces to the water flow. The brine tracer tests were performed after approximately 20 PV chase water injection with the same flow rate as in the gel injection. As illustrated in **Fig. 21,** the results showed that the tracer breakthrough occurred significantly earlier after gel injection. It indicated that the effective PV was reduced because the pore spaces were occupied by the gel particles.

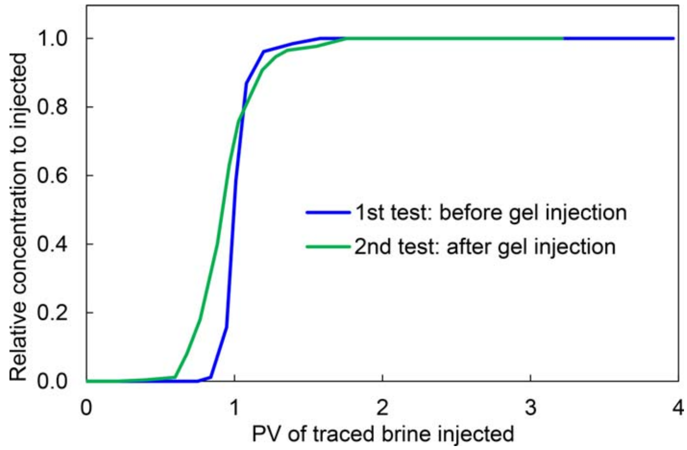

Fig. 21—Results of brine tracer test after gel injection (Exp. 1).

***Salinity-Responsive Behavior of* F_{rrw}.** Because the swelling behavior of the microgels was responsive to the salinity of brine, we wondered how the residual resistance factor would change when brines with different salinities were injected. A high-salinity water slug (formation brine, 27,500 ppm) was injected at the same flow rate after the first low-salinity chase water (i.e., injection brine, 2,498 ppm) to test the effect of salinity on the water blocking efficiency. The injection pressures and the residual resistance factors were significantly reduced **(Figs. 22 and 23).** Afterward, a second low-salinity water slug was injected at the same flow rate. Interestingly, the pressures and residual resistance factors were recovered almost to the same level as in the first low-salinity chase waterflood, as shown in Figs. 22 and 23. The results suggested that the gel would shrink when the high-salinity water was injected. The reason was that the high concentration of ions in the high-salinity water exerted higher compressive forces on the networks and polymer chains of the gels. Consequently, the gels lost water, and the volume was reduced (i.e., shrunk). The PV occupied by the gels was reduced, and wormholes or microchannels were generated through the gel bank. Thus, the resistance ability to the water flow was reduced, as indicated by the lower residual resistance factors during the high-salinity water injection in Fig. 23. Our observations also demonstrated that the shrinking and swelling properties of the microgels were reversible. The stability of gel materials was not destroyed by the alternate salinity environment. After injecting low-salinity water again, the concentration of surrounding ions was reduced, the compression forces applied on the networks of the gels were reduced, and thus, the screen effect was weakened. The polymer chains and the networks stretched, and more water was absorbed; thus, the gels reswelled. Consequently, the wormholes and microchannels created during the high-salinity waterflood were resealed, and the resistance ability was recovered. The salinity-responsive behavior was also observed by Brattekås et al. (2019) for Cr(III)-HPAM gel systems.

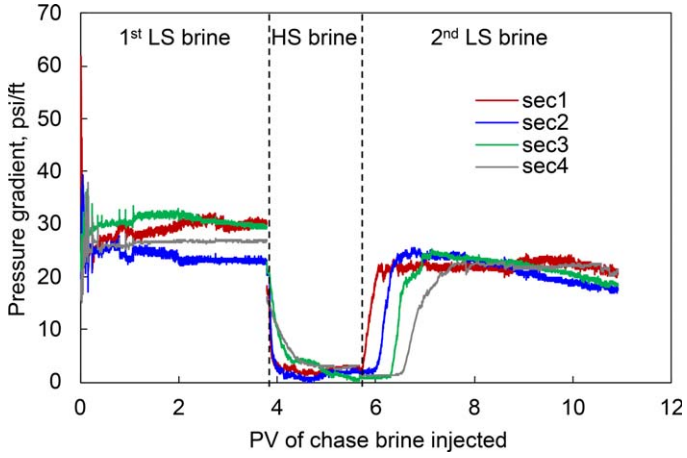

Fig. 22—Pressure gradient during post-waterflood at different salinities (Exp. 1). HS = high-salinity; LS = low-salinity.

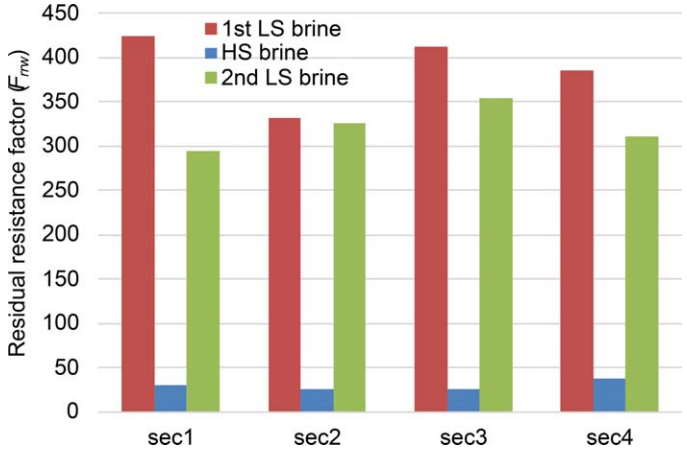

Fig. 23—Salinity-responsive behavior of residual resistance factor to water (Exp. 1). HS = high-salinity; LS = low-salinity; sec = section.

Can this particular behavior be used in fields? Taking Milne Point oil field as an example, the formation water has a high salinity of approximately 27,500 ppm, and in a normal waterflood or polymer flood, the salinity is much lower, approximately 2,500 ppm, less than one-tenth of the formation brine. Therefore, if the microgel is carried with high-salinity water, the particles placed in the formation can further swell during the post waterflooding or polymer flooding. The further swelling of the gel particles can result in a reinforced water blocking capacity in the channels and thus force the displacing fluid into the unswept zones (oil zones) to displace the previously bypassed oil. Thus, the sweep efficiency can be improved.

Disproportionate Permeability Reduction Effect of the Microgels. Crude oil was injected after the post-waterflood to test the blocking effect of the microgel bank to oil flow. The residual resistance factors were estimated based on the stable pressures at different locations of the sandpacks. Interestingly, the residual resistance factor to the oil flow was much lower than the residual resistance factor to the water flow (i.e., $F_{rrw} \gg F_{rro}$), as shown in **Fig. 24.** That is, the microgels reduced the permeability to the water flow much more than the permeability to the oil flow. This phenomenon was termed the DPR effect. The F_{rro} was in the range of 4.5 to 21, whereas the

F_{rrw} was in the range of 330 to 420. The F_{rrw} was approximately 20 to 92 times the F_{rro}. The DPR effect was also observed for bulk polymer gel systems (Liang et al. 1995; Al-Sharji et al. 1999; Willhite et al. 2002; Seright 2009) and PPG systems (Imqam et al. 2014). The DPR effect was also observed by Zhao et al. (2014) after treatment with dispersed particle gels they developed. Different mechanisms have been proposed in the literature to interpret the special phenomenon, and a brief summary can be found in the work of Alfarge et al. (2017).

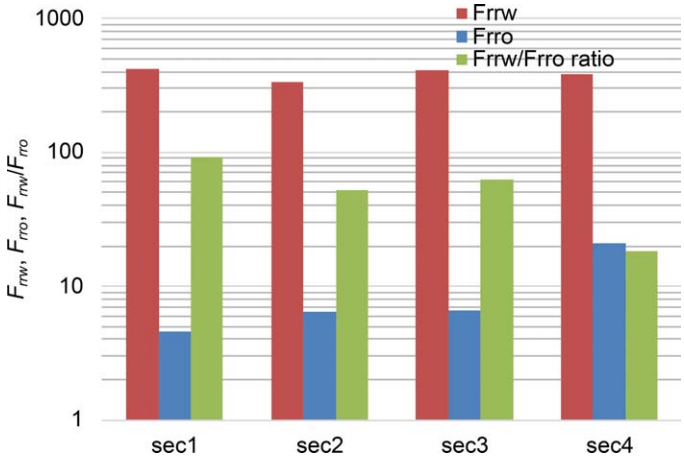

Fig. 24—DPR effect of the microgels. (The gels reduced the sandpack permeability to water flow much more than that to oil flow.) sec = section.

Conclusions

In this study, a series of experiments were carried out to investigate the transport behavior of microgels in super-K channels. Sandpacks with permeabilities ranging from 27 to 221 darcies were used to mimic the super-K channels. Multiple pressure sensors were applied along the sandpack models to monitor the propagation behavior of the microgels.

1. The tested microgel particles could transport through the super-K channels, and a higher driving pressure gradient was required when the particle/pore size ratio was larger. The pressure gradient distribution along the super-K channels was relatively uniform when the particle/pore ratio was low (less than 1.3). However, the inlet section would show increasingly higher-pressure gradients as the particle/pore ratio was increased, indicating increased difficulty in propagation.
2. The propagation of the gel particles was significantly slower compared with the carrying fluid. The delayed propagation behavior was more pronounced when the particle/pore ratio was higher.
3. The injection pressure was less sensitive to the injection flow rate compared with a Newtonian fluid. The gel dispersion exhibited an apparent shear thinning (pseudoplastic) behavior when transporting through the porous channels.
4. Breakage of the gel particles was observed especially at high superficial velocities. The particle breakage was partially responsible for the apparent shear thinning behavior. The breakage phenomenon is in favor of deep placement of the gel particles. On the other hand, the breakage behavior might reduce the blocking efficiency of the gels. This might be tolerable because the blocking ability in the in-depth regions does not need to be as strong as in the near-wellbore region.
5. The channel permeabilities were significantly reduced by the microgels, bringing sufficient resistance to subsequent waterflooding (more than 99.5%). At the given matching size conditions, softer gels are more likely to establish in-depth placement and uniform water blocking capacity in the channels. The microgel particles exhibit salinity-responsive behavior to the post-brine flush. This suggests that the gel particles can shrink and reswell according to the salinity of the injected water. Possibilities are discussed to use this salinity-responsive behavior.
6. The microgels exhibit a particular DPR effect. After gel injection, the channel permeability to water flow was reduced by more than 20 to 92 times the permeability to oil flow.

Nomenclature

d = average pore throat size
E_{bw} = water blocking efficiency
f_{CK} = Carman-Kozany shape factor
F_r = resistance factor
F_{rrw} = residual resistance factor
k = permeability
ΔP = differential pressure between the injector and the producer
λ = mobility
ϕ = porosity
τ = tortuosity

Acknowledgments

The financial support from U.S. Department of Energy and Hilcorp Alaska Award DE-FE0031606 are appreciated. This material is based upon work supported by the Department of Energy under Award DE-FE0031606.

References

Aldhaheri, M., Wei, M., Alhuraishawy, A. et al. 2021. Field Performances, Effective Times, and Economic Assessments of Polymer Gel Treatments in Controlling Excessive Water Production from Mature Oil Fields. *J Energy Resour Technol* **143** (8): 080804. https://doi.org/10.1115/1.4049019.

Aldhaheri, M., Wei, M., Zhang, N. et al. 2020. Field Design Guidelines for Gel Strengths of Profile-Control Gel Treatments Based on Reservoir Type. *J Pet Sci Eng* **194:** 107482. https://doi.org/10.1016/j.petrol.2020.107482.

Alfarge, D. K., Wei, M., and Bai, B. 2017. Numerical Simulation Study of Factors Affecting Relative Permeability Modification for Water-Shutoff Treatments. *Fuel* **207:** 226–239. https://doi.org/10.1016/j.fuel.2017.06.041.

Al-Ibadi, A. and Civan, F. 2013. Experimental Investigation and Correlation of Treatment in Weak and High-Permeability Formations by Use of Gel Particles. *SPE Prod & Oper* **28** (4): 387–401. SPE-153557-PA. https://doi.org/10.2118/153557-PA.

Al-Sharji, H. H., Grattoni, C. A., Dawe, R. A. et al. 1999. Pore-Scale Study of the Flow of Oil and Water through Polymer Gels. Paper presented at the SPE Annual Technical Conference and Exhibition, Houston, Texas, USA, 3–6 October. SPE-56738-MS. https://doi.org/10.2118/56738-MS.

Bai, B., Huang, F., Liu, Y. et al. 2008. Case Study on Preformed Particle Gel for In-Depth Fluid Diversion. Paper presented at the SPE Symposium on Improved Oil Recovery, Tulsa, Oklahoma, USA. SPE-113997-MS. https://doi.org/10.2118/113997-MS.

Bai, B., Li, L., Liu, Y. et al. 2007a. Preformed Particle Gel for Conformance Control: Factors Affecting Its Properties and Applications. *SPE Res Eval & Eng* **10** (4): 415–421. SPE-89389-PA. https://doi.org/10.2118/89389-PA.

Bai, B., Liu, Y., Coste, J. P. et al. 2007b. Preformed Particle Gel for Conformance Control: Transport Mechanism through Porous Media. *SPE Res Eval & Eng* **10** (2): 176–184. SPE-89468-PA. https://doi.org/10.2118/89468-PA.

Bai, B., Wei, M., and Liu, Y. 2012. Injecting Large Volumes of Preformed Particle Gel for Water Conformance Control. *Oil Gas Sci Technol–Rev IFP Energies Nouvelles* **67** (6): 941–952. https://doi.org/10.2516/ogst/2012058.

Bai, B., Wei, M., and Liu, Y. 2013. Field and Lab Experience with a Successful Preformed Particle Gel Conformance Control Technology. Paper presented at the SPE Production and Operations Symposium, Oklahoma City, Oklahoma, USA, 23–26 March. SPE-164511-MS. https://doi.org/10.2118/164511-MS.

Bai, B., Zhou, J., and Yin, M. 2015. A Comprehensive Review of Polyacrylamide Polymer Gels for Conformance Control. *Pet Explor Dev* **42** (4): 525–532. https://doi.org/10.1016/S1876-3804(15)30045-8.

Brattekås, B., Graue, A., and Seright, R. S. 2019. Low-Salinity Chase Waterfloods Improve Performance of Cr(III)-Acetate Hydrolyzed Polyacrylamide Gel in Fractured Cores. *SPE Res Eval & Eng* **19** (2): 331–339. SPE-173749-PA. https://doi.org/10.2118/173749-PA.

Carman, P. C. 1956. *Flow of Gases through Porous Media*. London, UK: Butterworths Scientific Publications.

Chang, H., Zhang, Y., Dandekar, A. et al. 2020. Experimental Investigation on Separation Behavior of Heavy-Oil Emulsion for Polymer Flooding on Alaska North Slope. *SPE Prod & Oper* **35** (3): 579–591. SPE-200369-PA. https://doi.org/10.2118/200369-PA.

Chauveteau, G., Tabary, R., Le Bon, C. et al. 2003. In-Depth Permeability Control by Adsorption of Weak Size-Controlled Microgels. Paper presented at the SPE European Formation Damage Conference, The Hague, The Netherlands, 13–14 May. SPE-82228-MS. https://doi.org/10.2118/82228-MS.

Dandekar, A., Bai, B., Barnes, J. et al. 2019. First Ever Polymer Flood Field Pilot: A Game Changer To Enhance the Recovery of Heavy Oils on Alaska's North Slope. Paper presented at the SPE Western Regional Meeting, San Jose, California, USA, 23–26 April. SPE-195257-MS. https://doi.org/10.2118/195257-MS.

Dandekar, A., Bai, B., Barnes, J. et al. 2021a. First Ever Polymer Flood Field Pilot To Enhance the Recovery of Heavy Oils on Alaska's North Slope–Pushing Ahead One Year Later. Paper presented at the SPE Western Regional Meeting, Virtual, 20–22 April. SPE-200814-MS. https://doi.org/10.2118/200814-MS.

Dandekar, A., Bai, B., Barnes, J. et al. 2021b. Heavy Oil Polymer EOR in the Challenging Alaskan Arctic: It Works! Paper presented at the Unconventional Resources Technology Conference, Houston, Texas, USA, 26–28 July. URTEC-2021-5077-MS. https://doi.org/10.15530/urtec-2021-5077.

Dhaliwal, A., Zhang, Y., Dandekar, A. et al. 2021. Experimental Investigation of Polymer Induced Fouling of Heater Tubes in the First-Ever Polymer Flood Pilot on Alaska North Slope. *SPE Prod & Oper* **36** (1): 70–82. SPE-200463-PA. https://doi.org/10.2118/200463-PA.

Elsharafi, M. O. and Bai, B. 2013. Minimizing Formation Damage for Preformed Particle Gels in Mature Reservoirs. Paper presented at the SPE Asia Pacific Enhanced Oil Recovery Conference, Kuala Lumpur, Malaysia, 11–13 August. SPE-174645-MS. https://doi.org/10.2118/174645-MS.

Elsharafi, M. O. and Bai, B. 2016. Influence of Strong Preformed Particle Gels on Low Permeable Formations in Mature Reservoirs. *Pet Sci* **13** (1): 77–90. https://doi.org/10.1007/s12182-015-0072-3.

Farasat, A., Sefti, M. V., Sadeghnejad, S. et al. 2017. Mechanical Entrapment Analysis of Enhanced Preformed Particle Gels (PPGs) in Mature Reservoirs. *J Pet Sci Eng* **157:** 441–450. https://doi.org/10.1016/j.petrol.2017.07.028.

Goudarzi, A., Zhang, H., Varavei, A. et al. 2015. A Laboratory and Simulation Study of Preformed Particle Gels for Water Conformance Control. *Fuel* **140:** 502–513. https://doi.org/10.1016/j.fuel.2014.09.081.

Imqam, A., Aldalfag, A., Wang, Y. et al. 2016. Evaluation of Preformed Particle Gels Penetration into Matrix for a Conformance Control Treatment in Partially Open Conduits. Paper presented at the SPE Annual Technology Conference and Exhibition, Dubai, UAE, 26–28 September. SPE-181545-MS. https://doi.org/10.2118/181545-MS.

Imqam, A., Bai, B., and Delshad, M. 2018. Micro-Particle Gel Transport Performance through Unconsolidated Sandstone and Its Blocking to Water Flow during Conformance Control Treatments. *Fuel* **231:** 479–488. https://doi.org/10.1016/j.fuel.2018.05.099.

Imqam, A., Bai, B., Xiong, C. et al. 2014. Characterizations of Disproportionate Permeability Reduction of Particle Gels through Fractures. Paper presented at the SPE Asia Pacific Oil & Gas Conference and Exhibition, Adelaide, Australia, 14–16 October. SPE-171531-MS. https://doi.org/10.2118/171531-MS.

Kang, W., Kang, X., Lashari, Z. A. et al. 2021. Progress of Polymer Gels for Conformance Control in Oilfield. *Adv Colloid Interface Sci* **289:** 102363. https://doi.org/10.1016/j.cis.2021.102363.

Larkin, R. J. and Creel, P. G. 2008. Methodologies and Solutions To Remediate Inner-Well Communication Problems on the SACROC CO2 EOR Project: A Case Study. Paper presented at the SPE Symposium on Improved Oil Recovery, Tulsa, Oklahoma, USA, 20–23 April. SPE-113305-MS. https://doi.org/10.2118/113305-MS.

Leng, J., Wei, M., and Bai, B. 2021. Review of Transport Mechanisms and Numerical Simulation Studies of Preformed Particle Gel for Conformance Control. *J Pet Sci Eng* **206:** 109051. https://doi.org/10.1016/j.petrol.2021.109051.

Li, J., Niu, L., and Lu, X. 2019. Migration Characteristics and Deep Profile Control Mechanism of Polymer Microspheres in Porous Media. *Energy Sci Eng* **7** (5): 2026–2045. https://doi.org/10.1002/ese3.409.

Liang, J.-T., Sun, H., and Seright, R. S. 1995. Why Do Gels Reduce Water Permeability More than Oil Permeability? *SPE Res Eng* **10** (4): 282–286. SPE-27829-PA. https://doi.org/10.2118/27829-PA.

Liu, Y., Bai, B., and Shuler, P. L. 2006. Application and Development of Chemical-Based Conformance Control Treatments in China Oil Fields. Paper presented at the SPE/DOE Symposium on Improved Oil Recovery, Tulsa, Oklahoma, USA, 22–26 April. SPE-99641-MS. https://doi.org/10.2118/99641-MS.

Liu, Y., Hou, J., Wang, Q. et al. 2017. Flow of Preformed Particle Gel through Porous Media: A Numerical Simulation Study Based on the Size Exclusion Theory. *Ind Eng Chem Res* **56** (10): 2840–2850. https://doi.org/10.1021/acs.iecr.6b03656.

Mauran, S., Rigaud, L., and Coudevylle, O. 2001. Application of the Carman-Kozeny Correlation to a High-Porosity and Anisotropic Consolidated Medium: The Compressed Expanded Natural Graphite. *Transp Porous Media* **43** (2): 355–376. https://doi.org/10.1023/A:1010735118136.

Ning, S., Barnes, J., Edwards, R. et al. 2020. First Ever Polymer Flood Field Pilot To Enhance the Recovery of Heavy Oils on Alaska North Slope: Producer Responses and Operational Lessons Learned. Paper presented at the SPE Annual Technical Conference and Exhibition, Virtual, 26–29 October. SPE-201279-MS. https://doi.org/10.2118/201279-MS.

Peirce, J. W., Hutcherson, M. R., Jensen, M. D. et al. 2014. An Overview of Conformance Control Efforts for the West Sak Field on the North Slope of Alaska. Paper presented at the SPE Improved Oil Recovery Symposium, Tulsa, Oklahoma, USA, 12–16 April. SPE-169073-MS. https://doi.org/10.2118/169073-MS.

Pyziak, D. and Smith, D. 2007. Update on Anton Irish Conformance Effort. Paper presented at the 6th International Conference on Production Optimization-Reservoir Conformance-Profile Control-Water and Gas Shutoff, Houston, Texas, USA, 6–7 November.

Saghafi, H. R. 2018. Retention Characteristics of Enhanced Preformed Particle Gels (PPGs) in Porous Media: Conformance Control Implications. *J Pet Sci Eng* **166:** 962–968. https://doi.org/10.1016/j.petrol.2018.03.098.

Seright, R. S. 1997. Use of Preformed Gels for Conformance Control in Fractured Systems. *SPE Prod & Fac* **12** (1): 59–65. SPE-35351-PA. https://doi.org/10.2118/35351-PA.

Seright, R. S. 1999a. Mechanism for Gel Propagation through Fractures. Paper presented at the SPE Rocky Mountain Regional Meeting, Gillette, Wyoming, USA, 15–18 May. SPE-55628-MS. https://doi.org/10.2118/55628-MS.

Seright, R. S. 1999b. Polymer Gel Dehydration during Extrusion through Fractures. *SPE Prod & Fac* **14** (2): 110–116. SPE-56126-PA. https://doi.org/10.2118/56126-PA.

Seright, R. S. 2001. Gel Propagation through Fractures. *SPE Prod & Fac* **16** (4): 225–231. SPE-74602-PA. https://doi.org/10.2118/74602-PA.

Seright, R. S. 2009. Disproportionate Permeability Reduction with Pore-Filling Gels. *SPE J*. **14** (1): 5–13. SPE-99443-PA. http://doi.org/10.2118/99443-PA.

Seright, R. S. and Brattekas, B. 2021. Water Shutoff and Conformance Improvement: An Introduction. *Pet Sci* **18** (2): 450–478. https://doi.org/10.1007/s12182-021-00546-1.

Seright, R. S., Lane, R. H., and Sydansk, R. D. 2003. A Strategy for Attacking Excess Water Production. *SPE Prod & Fac* **18** (3): 158–169. SPE-84966-PA. https://doi.org/10.2118/84966-PA.

Sydansk, R. D. and Romero-Zeron, L. 2011. *Reservoir Conformance Improvement*. Richardson, Texas, USA: Society of Petroleum Engineers.

Targac, G., Gallo, C., Smith, D. et al. 2020. Case History of Conformance Solutions for West Sak Wormhole/Void Space Conduit with a New Reassembling Pre-Formed Particle Gel RPPG. Paper presented at the SPE Annual Technical Conference and Exhibition, Virtual, 26–29 October. SPE-201302-MS. https://doi.org/10.2118/201302-MS.

Vasquez, J. E., Dalrymple, E. D., Abbasy, I. et al. 2008. Laboratory Evaluation of Water Swellable Materials for Fracture Shutoff. Paper presented at the SPE North Africa Technical Conference and Exhibition, Marrakech, Morocco, 12–14 March. SPE-111492-MS. https://doi.org/10.2118/111492-MS.

Villone, M. M. and Maffettone, P. L. 2019. Dynamics, Rheology, and Applications of Elastic Deformable Particle Suspensions: A Review. *Rheol Acta* **58** (3–4): 109–130. https://doi.org/10.1007/s00397-019-01134-2.

Wang, J., Zhang, H., Liu, H. et al. 2017. Quantification of Transportation of Deformable Gel Particles in Porous Media. Paper presented at the SPE Annual Technical Conference and Exhibition, San Antonio, Texas, USA, 9–11 October. SPE-187266-MS. https://doi.org/10.2118/187266-MS.

Willhite, G. P., Zhu, H., Natarajan, D. et al. 2002. Mechanisms Causing Disproportionate Permeability in Porous Media Treated with Chromium Acetate/HPAAM Gels. *SPE J*. **7** (1): 100–108. SPE-77185-PA. https://doi.org/10.2118/77185-PA.

Wu, D., Zhou, K., Hou, J. et al. 2021. Review of Experimental and Simulation Studies of Enhanced Oil Recovery Using Viscoelastic Particles. *J Dispers Sci Technol* **42** (7): 956–969. https://doi.org/10.1080/01932691.2020.1723620.

Yao, C., Lei, G., Cathles, L. M. et al. 2014. Pore-Scale Investigation of Micron-Size Polyacrylamide Elastic Microspheres (MPEMs) Transport and Retention in Saturated Porous Media. *Environ Sci Technol* **48** (9): 5329–5335. https://doi.org/10.1021/es500077s.

Yao, C., Lei, G., Li, L. et al. 2012. Selectivity of Pore-Scale Elastic Microspheres as a Novel Profile Control and Oil Displacement Agent. *Energ Fuel* **26** (8): 5092–5101. https://doi.org/10.1021/ef300689c.

Yao, C., Liu, B., Li, L. et al. 2020. Transport and Retention Behaviors of Deformable Polyacrylamide Microspheres in Convergent-Divergent Microchannels. *Environ Sci Technol* **54** (17): 10876–10884. https://doi.org/10.1021/acs.est.0c02243.

Yao, C., Wang, D., Wang, J. et al. 2017. Effect of Ionic Strength on the Transport and Retention of Polyacrylamide Microspheres in Reservoir Water Shutoff Treatment. *Ind Eng Chem Res* **56** (28): 8158–8168. https://doi.org/10.1021/acs.iecr.7b01588.

Zhao, G., Dai, C., and Zhao, M. 2014. Investigation of the Profile Control Mechanisms of Dispersed Particle Gel. *PLoS One* **9** (6): e100471. https://doi.org/10.1371/journal.pone.0100471.

Zhao, Y., Leng, J., Lin, B. et al. 2021a. Experimental Study of Microgel Conformance-Control Treatment for a Polymer-Flooding Reservoir Containing Superpermeable Channels. *SPE J*. **26** (4): 2305–2317. SPE-205486-PA. https://doi.org/10.2118/205486-PA.

Zhao, Y., Yin, S., Seright, R. S. et al. 2021b. Enhancing Heavy-Oil-Recovery Efficiency by Combining Low-Salinity-Water and Polymer Flooding. *SPE J*. **26** (3): 1535–1551. SPE-204220-PA. https://doi.org/10.2118/204220-PA.

Zhou, K., Hou, J., Sun, Q. et al. 2017. An Efficient LBM-DEM Simulation Method for Suspensions of Deformable Preformed Particle Gels. *Chem Eng Sci* **167:** 288–296. https://doi.org/10.1016/j.ces.2017.04.026.